Soham S. Mujumdar
Department of Mechanical
Science and Engineering,
University of Illinois at Urbana-Champaign,
Champaign, IL 61801
e-mail: mujumda2@illinois.edu

Davide Curreli
Assistant Professor
Department of Nuclear, Plasma
and Radiological Engineering,
University of Illinois at Urbana-Champaign,
Champaign, IL 61801
e-mail: dcurreli@illinois.edu

Shiv G. Kapoor[1]
Professor
Department of Mechanical
Science and Engineering,
University of Illinois at Urbana-Champaign,
Champaign, IL 61801
e-mail: sgkapoor@illinois.edu

David Ruzic
Professor
Center for Plasma-Material Interactions,
Department of Nuclear, Plasma
and Radiological Engineering,
University of Illinois at Urbana-Champaign,
Champaign, IL 61801
e-mail: druzic@illinois.edu

Model-Based Prediction of Plasma Resistance, and Discharge Voltage and Current Waveforms in Micro-Electrodischarge Machining

In electrodischarge machining (EDM), the thermal energy causing material removal at the electrodes is given by the electrical energy supplied to the discharge. This electrical energy, also known as the discharge energy, can be obtained from time-transient voltage and current waveforms across the electrodes during a discharge. However, in micro-EDM, the interelectrode gaps are shorter causing the plasma resistance to be significantly smaller than other impedances in the circuit. As a result, the voltage and current waveforms obtained by a direct measurement may include voltage drop across the stray impedances in the circuit and may not accurately represent the exact voltage drop across micro-EDM plasma alone. Therefore, a model-based approach is presented in this paper to predict time-transient electrical characteristics of a micro-EDM discharge, such as plasma resistance, voltage, current, and discharge energy. A global modeling approach is employed to solve equations of mass and energy conservations, dynamics of the plasma growth, and the plasma current equation for obtaining a complete temporal description of the plasma during the discharge duration. The model is validated against single-discharge micro-EDM experiments and then used to study the effect of applied open gap voltage and interelectrode gap distance on the plasma resistance, voltage, current, and discharge energy. For open gap voltage in the range of 100–300 V and gap distance in the range of 0.5–6 μm, the model predicts the use of a higher open gap voltage and a higher gap distance to achieve a higher discharge energy. [DOI: 10.1115/1.4031773]

1 Introduction

EDM is a machining process that utilizes electrical discharges between two electrodes that are separated by a small gap filled with dielectric liquid. When a sufficient voltage is applied between the electrodes, initial resistance of the interelectrode gap decreases rapidly as the current in the gap increases to form a highly conductive plasma channel. The plasma contains high energy ions and electrons that cause electrode erosion via melting and evaporation. It is the electrical resistance of the plasma along with the circuit current that dictates the evolution of interelectrode voltage (i.e., discharge voltage) and more importantly, the amount of electrical energy going into a discharge. During a discharge, this electrical energy is converted into a thermal energy of ions and electrons to cause material removal and can be manipulated to maximize the material removal rate (MRR) [1–4]. The shape of discharge voltage and current waveforms can also be used to sense the interelectrode gap conditions during a machining operation and control the electrode feed for greater stability and productivity [5,6]. Therefore, it is important to study the dynamics of the plasma resistance and subsequent evolution of discharge voltage and current waveforms in order to understand the material removal mechanism in EDM and achieve higher productivity.

The information about the transient resistance of the plasma and the energy of the discharge can be obtained, in principle, from the discharge voltage and current waveforms that are commonly measured during an EDM operation [5–8]. However, in micro-EDM, the interelectrode gaps (1–10 μm) are much shorter compared to conventional EDM. Therefore, the plasma resistance during a discharge is very small and comparable to the other resistive and reactive components in the EDM circuit. As a result, the voltage and current waveforms obtained by a direct measurement may not accurately represent the actual plasma voltage/current due to any stray circuit impedance between the plasma and the point of measurement. Due to physical limitations on how close to the actual discharge location the measurement can be obtained, the measured voltage will always be much higher than the actual plasma voltage, thereby, leading to an overestimation of the discharge power. Also, sensitivity of the measurement device may not be sufficient to capture the rapid collapse of the interelectrode voltage during narrower pulse-widths (<10 μs) [8]. A model-based approach, however, can prove to be helpful in this case to obtain a more accurate estimation of voltage and current characteristics of the discharge. With this purpose, many attempts have been made by researchers to model the transient behavior of high-voltage underwater discharges [8–11]. However, there is a lack of such modeling efforts in the case of micro-EDM plasma. A typical micro-EDM plasma is characterized by shorter interelectrode gaps (1–10 μm), lower discharge energies, and narrower pulse-widths (up to 10 μs). Therefore, models for the high-voltage underwater discharges cannot be applied to micro-EDM plasma.

The purpose of this paper is to predict the time-transient behavior of micro-EDM plasma resistance and thereby, obtain accurate information about the time-transient plasma voltage/current waveforms and the discharge energy, which plays a crucial part in material removal. A 0D plasma model developed earlier by the authors [12] is used to model the micro-EDM plasma. The model

[1]Corresponding author.

Contributed by the Manufacturing Engineering Division of ASME for publication in the Journal of Micro- and Nano-Manufacturing. Manuscript received July 2, 2015; final manuscript received October 7, 2015; published online October 29, 2015. Assoc. Editor: Bin Wei.

is further enhanced by adding the physics of plasma resistance and a new electrical circuit solver module to solve for the currents in the discharge circuit.

The rest of the paper is divided as follows: The formulation of the enhanced plasma model [12] is discussed first in Sec. 2. Model evaluation and experimental validation of the model-based electrical characteristics of the plasma are presented in Sec. 3. Results of the plasma model for a variety of discharge conditions are discussed in Sec. 4 followed by conclusions in Sec. 5.

2 Model Formulation

To model the electrical characteristics of the micro-EDM plasma, a new electrical circuit solving module is added to the previously developed micro-EDM plasma model [12]. The micro-EDM plasma model uses a global modeling approach that assumes a spatially uniform plasma (0D) in the gap to predict time-transient characteristics of the plasma. A complete description of the micro-EDM plasma offered by 0D plasma model such as discussed in Ref. [12] is necessary to predict the electrical resistance of the plasma because characteristics of the plasma, such as plasma composition, temperature, size, and plasma resistance, are interdependent. The plasma resistance during a discharge is a function of time-varying electron density of the plasma and the size of the plasma. In a dielectric, like deionized (DI) water, the electrons are generated by dissociation and ionization of H_2O molecule into different atoms/molecules/ions and their subsequent chemical interactions. The reaction rates of the chemical reactions of these species are functions of the plasma temperature that again depends on the electrical energy going into a discharge. Figure 1 presents the schematic of the 0D micro-EDM plasma model [12]. As shown in the figure, the enhanced model consists of four modules, namely, plasma chemistry, power balance, plasma bubble dynamics, and a new electrical circuit solver module. With the help of plasma chemistry, power balance, and plasma bubble dynamics modules, the model solves simple equations of mass conservation and energy conservation along with plasma bubble dynamics to predict first-hand estimates of time-transient plasma characteristics, such as plasma composition, density, plasma temperature, radius, pressure, and the heat flux to electrodes. By addition of a new electrical circuit solver module, the model can also predict the evolution of plasma resistance, voltage/current waveforms, and amount of discharge energy, which was not possible previously with the original model. This also eliminates the need to provide the voltage and current waveform measurements from the experiments as an input to the model, thereby, improving the predictive power of the plasma model. A brief description of each of these modules is given below. More details about the mathematical formulation of the model can be obtained in Ref. [12].

2.1 Plasma Chemistry. As H_2O is a triatomic molecule, there is a multitude of possible reactions and different chemical pathways (combination of reactions leasing to same product) in its plasma phase. The plasma chemistry module solves for the concentrations of different neutral and ionic species in the plasma by considering the chemical kinetics of these reactions. For computational simplicity, a set of 41 dominant reactions involving 19 species have been considered in this model. The list of all the species and the temperature-dependent reaction rates used in this model can be found in Ref. [12]. In the H_2O plasma, recombination and charge transfer reactions dominate at lower temperatures of the reactants ($T < 10{,}000$ K), while at higher temperatures ($T > 10{,}000$ K), dissociation and ionization reactions become dominant.

2.2 Power Balance. Temperature of the species is given by the power balance module. Since the electrons have significantly smaller mass than all the other species in the plasma, a separate temperature (T_e) is assigned to electrons, while the rest of the species are assumed to be at the same temperature (T_g). The power balance module, therefore, solves two separate power balance equations, one for the electrons and another for rest of the species by balancing the electrical power input with losses via radiation, elastic/inelastic collisions, mechanical work in plasma expansion, etc.

2.3 Plasma Bubble Dynamics. To predict the growth of the plasma channel, plasma is assumed to be a spherical bubble in shape and growth of the plasma bubble is modeled using Kirkwood–Bethe approximation in the bubble dynamics module. The bubble dynamic model solves for the radius and speed of expansion of the plasma bubble during the discharge. The radius of the plasma bubble determines the area of the plasma in contact with the workpiece, which is crucial for calculating the resistance of the plasma channel as discussed in Sec. 2.4. More details about the formulation of plasma bubble dynamics can be found in Ref. [12].

2.4 Electrical Circuit Solver. To model the voltage and current during a micro-EDM plasma discharge, electrical circuit solver module was added to the existing plasma model. This module solves equations for the electrical circuit that generates the voltage pulse to the electrodes. A transistor-based resistor-capacitor (RC) discharge circuit typically used for micro-EDM is shown in Fig. 2(*a*). This circuit uses an metal-oxide-semiconductor field-effect transistor (MOSFET) to control the pulse-width of the voltage pulse provided by an RC discharge. After accounting for the impedances in the circuit due to component structure and wiring, an equivalent circuit is shown in Fig. 2(*b*). In the equivalent circuit, the plasma is assumed to be a simple resistor element with time-varying resistance as it evolves during the discharge. Other

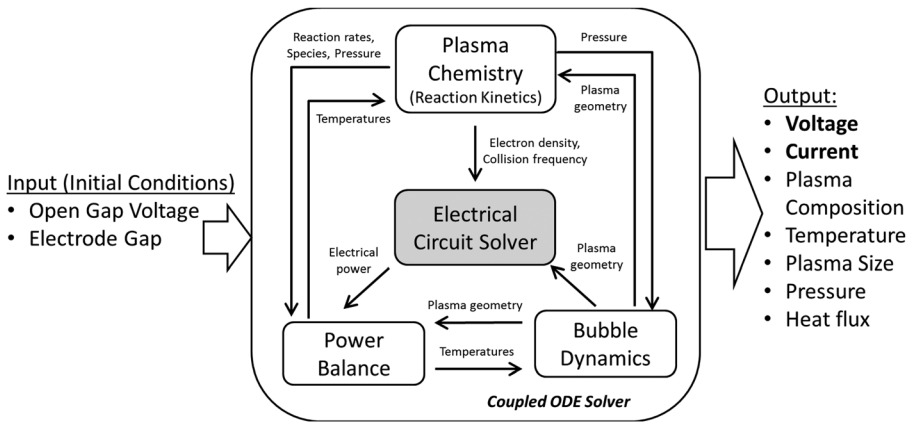

Fig. 1 Schematic of the enhanced micro-EDM plasma model formulation

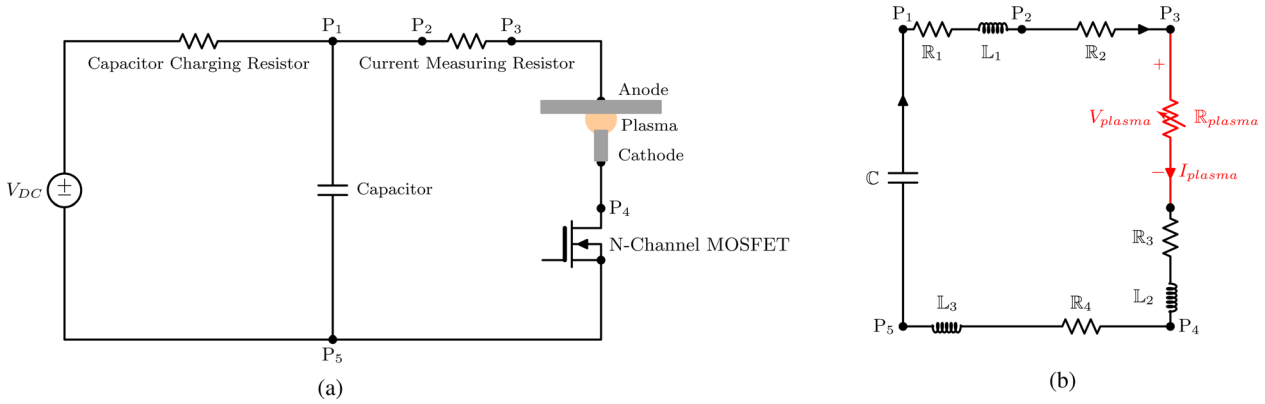

Fig. 2 Schematic of the electrical circuit used for micro-EDM: (*a*) hybrid RC-transistor circuit for micro-EDM and (*b*) equivalent discharge circuit showing all the circuit components

impedances in the circuit are modeled as resistor and inductor elements in series.

To calculate the plasma resistance, direct current (DC) conductivity (σ_{DC} (S/m)) of the plasma (H_2O plasma in this case) is determined first using cold plasma approximation [13]

$$\sigma_{DC} = \frac{e^2 n_e}{m_e \nu_{m,e}} \tag{1}$$

where e (C) is the electronic charge, n_e (m^{-3}) is the number density of electrons, m_e (kg) is the electronic mass, and $\nu_{m,e}$ (s^{-1}) is the collision frequency of the electrons with neutrals. As the conductivity of the plasma is directly proportional to electron density, it changes as the electron density changes during the discharge. From the conductivity, a resistance of the plasma ($\mathbb{R}_{plasma}$ (Ω)) is obtained by a simple approximation

$$\mathbb{R}_{plasma} = \left(\frac{1}{\sigma_{DC}}\right)\left(\frac{L}{A_w}\right) = \left(\frac{m_e \nu_{m,e}}{e^2 n_e}\right)\left(\frac{L}{A_w}\right) \tag{2}$$

where L (m) is the interelectrode gap distance and A_w (m^2) is the area of workpiece (anode) in contact with the plasma bubble given by plasma bubble dynamics module. Now, the equations solving for plasma current (I_{plasma} (A)) and plasma voltage (V_{plasma} (V)) can be written for the equivalent circuit shown in Fig. 2(*b*) as

$$I_{plasma} = \frac{dQ}{dt} \tag{3}$$

$$\begin{aligned} V_{plasma} &= I_{plasma} \times \mathbb{R}_{plasma} \\ &= \frac{Q}{\mathbb{C}} - (\mathbb{R}_1 + \mathbb{R}_2 + \mathbb{R}_3 + \mathbb{R}_4) I_{plasma} \\ &\quad -(\mathbb{L}_1 + \mathbb{L}_2 + \mathbb{L}_3)\frac{dI_{plasma}}{dt} \end{aligned} \tag{4}$$

where $\mathbb{R}_i$ (Ω) and $\mathbb{L}_i$ (H) are the resistances and inductances in the circuit (refer to Fig. 2(*b*)), respectively. $\mathbb{C}$ (F) is the capacitance and Q (C) is the charge in the circuit. Equations (3) and (4) are rearranged as ordinary differential equations (ODEs) in variable Q and are then solved simultaneously with ODEs from other modules of the plasma model [12].

3 Model Evaluation and Validation

To evaluate the model, the micro-EDM circuit used to generate the discharge voltage (refer to Fig. 2(*a*)) was characterized first. Using an LCR meter (Instek LCR-817) and a TENMA 72-8150 electrical meter, initial estimates of the different circuit components, i.e., $\mathbb{R}_1, \mathbb{R}_2, \mathbb{R}_3, \mathbb{R}_4, \mathbb{L}_1, \mathbb{L}_2$, and $\mathbb{L}_3$, of the equivalent circuit shown in Fig. 2(*b*) were obtained. During this exercise, the electrodes were assumed to be in short-circuit condition, i.e., in electrical contact with each other such that $\mathbb{R}_{plasma} = 0$ (refer to Fig. 2). Gray-box model estimation toolbox of MATLAB [14] was then used for each pair of points in the circuit including (P_1, P_2), (P_3, P_4), and (P_4, P_5) to obtain the final estimates of these resistances and inductances. For example, to obtain the values of $\mathbb{R}_1$ and $\mathbb{L}_1$, a simple ordinary differential equation was written for circuit path between the points P_1 and P_2 as

$$\frac{dI_{short}}{dt} = -\frac{\mathbb{R}_1}{\mathbb{L}_1} I_{short} + \frac{1}{\mathbb{L}_1} V_{1,2} \tag{5}$$

Here, I_{short} denotes the current in the circuit shown in Fig. 2(*b*) in short-circuit condition, i.e., when $\mathbb{R}_{plasma} = 0$ and $V_{1,2}$ is the voltage across points P_1 and P_2. The time-dependent waveform of $V_{1,2}$ was obtained experimentally by sending a 100 V pulse with pulse-on-time of 5 μs in the circuit and measuring the voltage drop across points P_1 and P_2. The current in the circuit (I_{short}) was also measured by measuring voltage drop across resistance ($\mathbb{R}_2$) between points P_2 and P_3 with initial estimate of $\mathbb{R}_2 = 0.60\,\Omega$. Treating the experimental value of $V_{1,2}$ as the input and experimental value of I_{short} as the output in Eq. (5), linear gray-box model estimation tool in MATLAB was used to estimate the values of $\mathbb{R}_1$ and $\mathbb{L}_1$. The values of $\mathbb{R}_1$ and $\mathbb{L}_1$ obtained from the direct measurement were used as an initial guess to arrive at final estimates of $\mathbb{R}_1$ and $\mathbb{L}_1$ such that the value of I_{short} obtained by Eq. (5) matches with the experimental measurement of I_{short} (normalized root-mean-square error $<1\%$). Using a similar procedure, the final estimates of $\mathbb{R}_3$, $\mathbb{L}_2$, $\mathbb{R}_4$, and $\mathbb{L}_3$ were obtained as well. The final values of all the circuit components are given in Table 1.

With known circuit parameters and given machining conditions, i.e., open gap voltage (V_0), interelectrode gap distance (L), and initial dielectric conductivity ($\sigma_{dc,0}$); the ODEs from plasma chemistry, power balance, plasma bubble dynamics, and electrical circuit solver modules were solved in coupled-manner to obtain evolution of plasma characteristics, i.e., plasma composition, plasma temperature, radius, pressure, and heat flux to electrodes along with plasma voltage and current. Details of the ODEs used in the plasma chemistry, power balance, and plasma bubble dynamics modules can be obtained in Ref. [12].

To validate the model, single-discharge experiments were carried out on a customized micro-EDM setup consisting of a hybrid

Table 1 Measured values of micro-EDM circuit components

$\mathbb{R}_1 = 0.286\ \Omega$	$\mathbb{C} = 551\ \mu F$
$\mathbb{R}_2 = 0.60\ \Omega$	$\mathbb{L}_1 = 1.15\ \mu H$
$\mathbb{R}_3 = 0.220\ \Omega$	$\mathbb{L}_2 = 2.05\ \mu H$
$\mathbb{R}_4 = 0.270\ \Omega$	$\mathbb{L}_3 = 1.20\ \mu H$

RC-transistor based circuit shown in Fig. 2(*a*). A tungsten rod with 500 μm diameter was used as tool electrode (cathode), titanium grade-5 alloy was used as the workpiece (anode), and DI water was used as the dielectric medium. The values of different process parameters, such as open gap voltage, interelectrode gap, initial DI water conductivity, and pulse-on-time, were chosen from a range of values typically used in micro-EDM [15,16] and were kept same for experiments and model evaluation, i.e., $V_0 = 100\,V$, $L = 1\,\mu$m, $\sigma_{dc,0} = 10\,\mu$S/cm, and $t_d = 5\,\mu$s. Voltage and current waveforms for the discharge were collected during each experimental trial using a 2 G samples/s Tektronix TDS2024B oscilloscope. To measure the discharge voltage, voltage across points P_3 and P_4 shown in Fig. 2(*a*) was collected and to measure the current, voltage drop across points P_2 and P_3 was collected. Points P_3 and P_4 are points in the circuit, which are directly connected to the electrodes by means of a long electrical wires. As discussed previously, the voltage measured across points P_3 and P_4 is not the actual discharge voltage due to stray impedances ($\mathbb{R}_3$ and $\mathbb{L}_2$) corresponding to the wiring between these points (refer to Fig. 2(*b*)) and the actual plasma. By measuring the stray impedances between the measurement points, voltage drop across P_3 and P_4, i.e., $V_{3,4}$, was simulated using the model and then compared with the experimental value. Similarly, model prediction of plasma current was compared with the experimental measurement of current obtained by dividing voltage drop across P_2 and P_3 by $\mathbb{R}_2$. The comparison plots of model prediction and experimental data with mean ± standard deviation from 15 trials have been shown in Fig. 3. It can be seen from Figs. 3(*a*) and 3(*b*) that the model predictions of $V_{3,4}$ and plasma current match reasonable well with the experimental measurement.

As the resistance of the plasma during the discharge is very small, it is difficult to obtain a direct measurement of the exact voltage drop across the tips of the electrode. Therefore, to obtain actual plasma voltage during a discharge, separate experimental trials were conducted by sending 100 V voltage pulse with pulse-on-time of 5 μs through the circuit in short-circuit condition, i.e., with EDM electrodes in contact with each other. Measurements of the voltage across points P_3 and P_4 ($V_{3,4,\text{short}}$) and the circuit current (I_{short}) during these trials were then used along with the corresponding voltage and current measurements ($V_{3,4}$, $I_{\text{plasma, exp}}$) from micro-EDM trials with open gap voltage of 100 V, interelectrode gap of 1 μm, and pulse-on-time of 5 μs to estimate experimental value of plasma resistance ($\mathbb{R}_{\text{plasma, exp}}$) and plasma voltage ($V_{\text{plasma, exp}}$) as

$$\mathbb{R}_{\text{plasma, exp}} = \frac{V_{3,4}}{I_{\text{plasma, exp}}} - \frac{V_{3,4,\text{ short}}}{I_{\text{short}}} \tag{6}$$

$$V_{\text{plasma, exp}} = \mathbb{R}_{\text{plasma, exp}} \times I_{\text{plasma, exp}} \tag{7}$$

Figures 3(*c*) and 3(*d*) compare the model predictions of the plasma voltage and resistance with the corresponding experimental measurements. It can be seen from Figs. 3(*c*) and 3(*d*) that the model predictions of plasma voltage and resistance lie within the limits of experimental error and capture the trends reasonably well. The mean values of the experimental plasma voltage and resistance are seen to be slightly higher than the model predictions, which can be attributed to the assumption of a spatially uniform plasma in the model. Note that the actual electrical discharge in water is spatially nonuniform with the plasma channel concentrated at the center of a larger water vapor bubble surrounding the plasma [17,18]. This may give rise to a higher plasma resistance than estimated from the model prediction. Figures 3(*c*) and 3(*d*) also show large errors (± standard deviation) about the mean values of experimental plasma voltage and plasma resistance, which can be attributed to the limitation on the signal-to-noise ratio of the oscilloscope used for the measurements.

4 Results and Discussion

The enhanced micro-EDM plasma model discussed in Sec. 2 can be used to simulate the plasma characteristics, such as plasma composition, temperature, pressure, radius, and heat flux along with the plasma electrical characteristics, i.e., resistance, voltage/current waveforms and discharge energy, during a micro-EDM

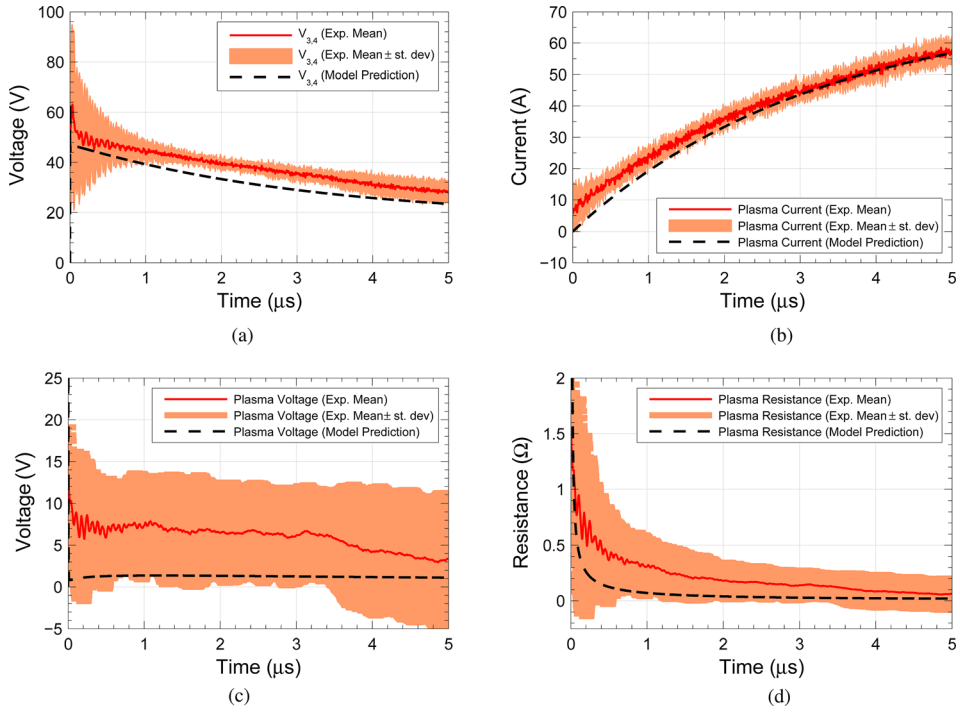

Fig. 3 Comparison of model prediction of voltage, current, and plasma resistance waveforms with the experimental measurements: (*a*) voltage across P_3 and P_4, (*b*) plasma current, (*c*) plasma voltage, and (*d*) plasma resistance

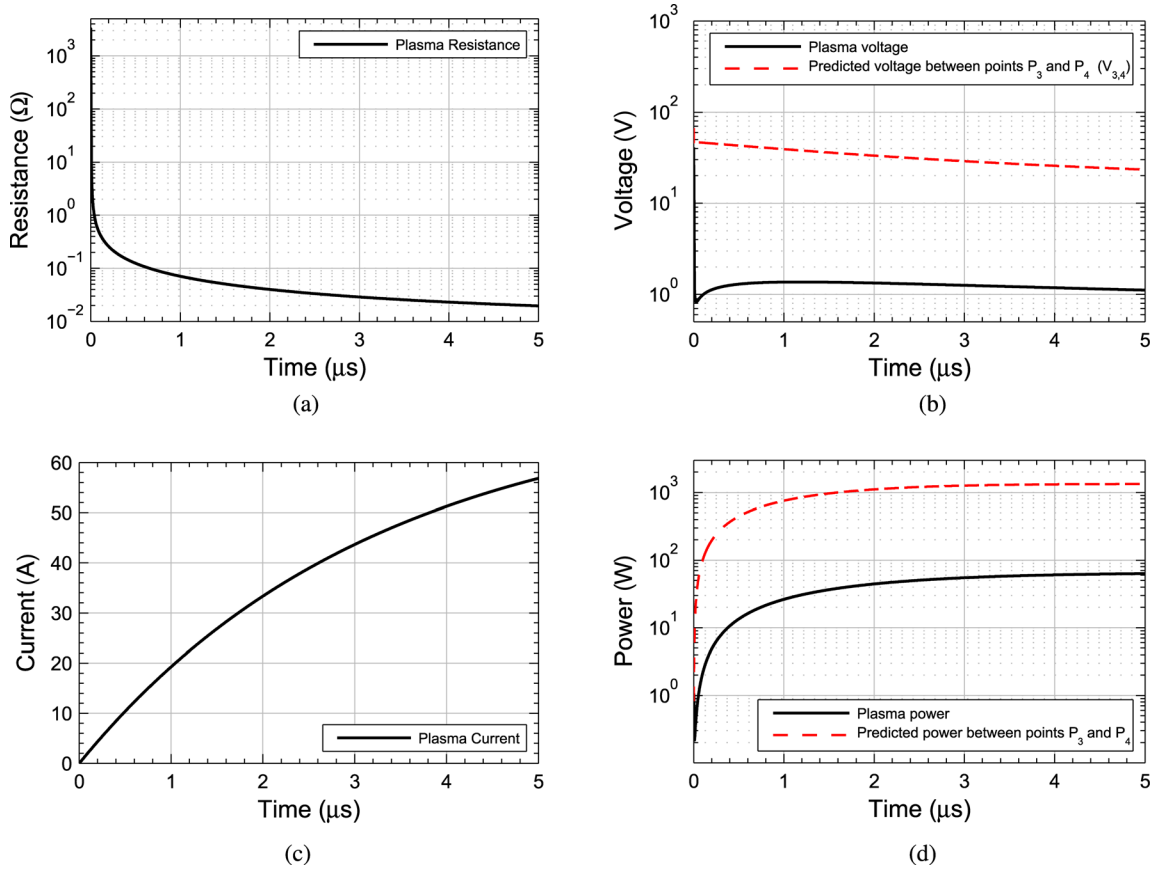

Fig. 4 Model-predicted evolution of electrical characteristics of a typical micro-EDM plasma ($V_0 = 100$ V and $L = 1$ μm): (*a*) plasma resistance, (*b*) voltage, (*c*) plasma current, and (*d*) power

discharge. The voltage and current waveforms present information of the time-transient plasma voltage and current that are otherwise difficult to obtain via direct measurements. The results of electrical characteristics of the plasma, viz., plasma voltage, current, resistance, and power, have been discussed in Sec. 4.1 first followed by a discussion on how the key micro-EDM process parameters, such as open gap voltage and gap distance, affect plasma resistance, voltage, current, and discharge energy of a single discharge in Sec. 4.2. Understanding the effect of open gap voltage and gap distance on the discharge energy can aid in maximizing the discharge energy of micro-EDM for enhanced productivity.

4.1 Evolution of the Electrical Characteristics During a Typical Discharge. For a typical micro-EDM discharge with $V_0 = 100$ V, $L = 1$ μm, and $\sigma_{dc,0} = 10$ μS/cm, time-evolution of the electrical characteristics of plasma, i.e., plasma voltage, current, resistance, and power, is plotted in Fig. 4. The discharge is simulated for discharge duration of $t_d = 5$ μs. Time-averaged values of the electrical characteristics are tabulated in Table 2. From Eqs. (1)–(4), it is clear that the resistance of the plasma is governed by evolution of the electron density and size of the plasma during the discharge. During a typical micro-EDM discharge, electron density of the plasma shows a steep increase within first few nanoseconds to its maximum value before starting to decay slowly as the discharge progresses [12]. At the same time, due to pressure created by various ionic/neutral species formed by dissociation and ionization of the water molecule; the plasma bubble continues to expand radially outward, which increases its area of contact (A_w) with the workpiece. Therefore, during the first few nanoseconds, increase in electron density as well as the plasma bubble size cause the resistance of the plasma to collapse rapidly as shown in Fig. 4(*a*). However, once the electron density starts to decay from its peak value, resistance of the plasma shows a gradual decrease in its value for most of the discharge duration.

Figure 4(*c*) shows that as the resistance of plasma drops due to formation of plasma channel, a plasma current is established in the interelectrode gap and it continues to grow as the resistance decreases. Model predicts plasma resistance of 20 mΩ at the end of discharge duration of 5 μs, while the maximum current in the plasma channel reaches ≈57 A at the end of the discharge. Due to a drop in resistance, the discharge voltage, i.e., plasma voltage, is seen to drop from initial open gap voltage of $V_0 = 100$ V to about 1.11 V at the end of 5 μs. Figure 4(*b*) also depicts the model-predicted voltage drop across points P_3 and P_4 in the circuit (Fig. 2(*b*)) since an experimental measurement is typically obtained away from the electrodes, such as across points P_3 and P_4. Comparing the model-predicted voltage across points P_3 and P_4 to the plasma voltage in Fig. 4(*b*) suggests that a voltage measurement obtained experimentally can overestimate the plasma voltage by almost one to two orders of magnitudes. Using the waveforms of voltage and current, electrical power going into a discharge is plotted against time as shown in Fig. 4(*d*) and it shows that the plasma power is much less than the predicted power across points P_3 and P_4. To obtain electrical energy of a

Table 2 Result of the micro-EDM plasma simulation for $V_0 = 100$ V, $L = 1$ μm, and $t_d = 5$ μs

Parameter	Maximum	Time-averaged	Minimum
Plasma voltage (V)	100[a]	1.28	1.11
Plasma current (A)	56.83	35.47	0[a]
Plasma resistance (Ω)	2433[a]	1.75	0.02
Discharge energy = 220 μJ			

[a]At the beginning of the discharge.

Table 3 Levels of open gap voltage (V_0) and gap used for simulation experiments

Process parameter	Levels
Open gap voltage (V)	100, 150, 200, 300
Gap (μm)	0.5, 1, 1.5, 2, 3, 4, 5, 6

discharge, numerical integration of the electrical power can be performed, which suggests that the discharge energy for the typical discharge is 220 μJ as compared to predicted value of 5200 μJ across points P_3 and P_4.

4.2 Effect of Open Gap Voltage and Gap Distance on Plasma Electrical Characteristics: Resistance, Voltage, Current, and Discharge Energy. In micro-EDM, the thermal energy causing electrode erosion comes from the electrical energy during a discharge. This electrical energy, also known as the plasma discharge energy, is a result of time-transient plasma voltage and current waveforms that are developed due to evolution of the plasma resistance during the discharge. Therefore, to understand the mechanism of material removal in micro-EDM, knowledge of the electrical characteristics of the micro-EDM plasma, i.e., plasma resistance, plasma voltage, plasma current, and the discharge energy, is essential. To study the effect of key micro-EDM process parameters, such as open gap voltage and gap distance, on these electrical characteristics, simulation experiments were designed with four levels of open gap voltage (V_0) and eight levels of interelectrode gap distance. The levels for these parameters are chosen so as to cover a wide range of open gap voltages and gap values typically used in micro-EDM and are tabulated in Table 3.

As seen from Fig. 4(*a*), the plasma resistance value shows a rapid collapse during first microsecond of the discharge before settling down to a smaller value for the rest of the discharge duration. The plasma voltage too, shown in Fig. 4(*b*), follows a similar trend. The plasma current, however, shows a continuous increase before reaching to its maximum value at the end of the discharge (see Fig. 4(*c*)). Therefore, to characterize the time-transient waveforms of the plasma resistance and the plasma voltage, their final value (at $t = 5\ \mu$s) is used, while the plasma current waveform is characterized by its time-averaged value during the discharge. Figure 5(*a*) shows the effect of open gap voltage and gap distance on the final plasma resistance. As seen from the figure, higher gap distance increases the resistance of the plasma during a discharge for a given open gap voltage. This is due to the combined effect of electron density, size of the plasma, and the gap distance. Increase in the gap distance increases the electron number density [12], however, decreases the radius of the plasma. As seen from Eq. (2), the resistance of the plasma is directly proportional to gap distance and inversely proportional to the size of the plasma and electron density. Therefore, as gap distance increases, the plasma resistance increases for a given open gap voltage. However, for a given gap distance, increase in open gap voltage decreases the resistance. This can be explained by the fact that as voltage is increased, both electron density and plasma size increase [12] causing resistance of the plasma to drop according to Eq. (2).

Figure 5(*b*) presents the effect of the open gap voltage and gap distance on the time-averaged plasma current. For a given open gap voltage, it can be seen that the value of plasma current does not show any appreciable change as the gap distance increases. This is because the resistance of the plasma, as seen from

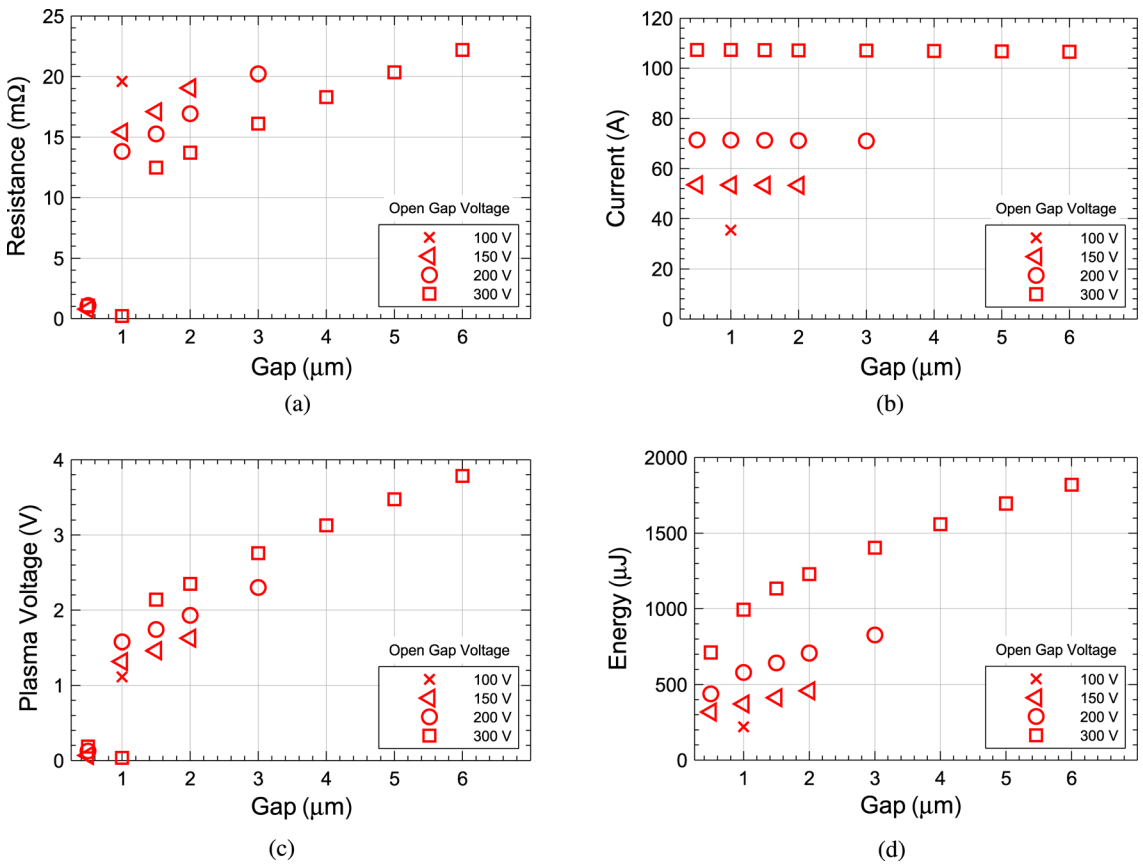

Fig. 5 Effect of open gap voltage and interelectrode gap distance on the electrical characteristics of micro-EDM plasma: (*a*) final plasma resistance (i.e., at $t = 5\ \mu$s), (*b*) time-averaged plasma current from $t = 0$ to $t = 5\ \mu$s, (*c*) final plasma voltage (i.e., at $t = 5\ \mu$s), and (*d*) discharge energy

Fig. 5(*a*), is approximately two orders of magnitude smaller than other resistances in the circuit (Table 1). Therefore, for all practical purposes, the total resistance of the circuit remains at near-constant value regardless of the changes in the plasma resistance. As a result, an increase in the plasma resistance following an increase in the gap distance does not significantly affect the value of the current in the circuit for a given open gap voltage. However, the plasma current increases when a higher open gap voltage is applied due to Ohm's law ($I = (V/R)$). Figure 5(*c*) presents the effect of open gap voltage and gap distance on the plasma voltage that can be obtained by product of the plasma resistance and the current. The plasma voltage increases with increase in the gap distance for a given open gap voltage and also with an increase in the open gap voltage for a given gap distance.

Finally, Fig. 5(*d*) presents the effect of open gap voltage and gap distance on the discharge energy of the plasma. When the gap distance is increased for a given open gap voltage, plasma current stays almost constant, while plasma resistance increases. Therefore, as shown in Fig. 5(*a*), discharge energy of the plasma increases with an increase in the gap distance following Ohmic (J) heating law (energy $\propto I^2 \mathbb{R}_{\text{plasma}}$). On the other hand, when the applied open gap voltage is increased at a given gap distance, plasma resistance decreases but current increases. As a combined result, the discharge energy of micro-EDM plasma is seen to increase with an increase in the open gap voltage when gap distance is held constant. Many experimental studies have shown that a higher discharge energy results in a higher MRR in EDM [15,19–23].

5 Conclusions

This paper explains development of an enhanced micro-EDM plasma model in DI water. A new electrical circuit solver module was added to the recently developed plasma model [12] to solve for time-transient electrical characteristics of the plasma, such as plasma resistance, plasma voltage, and current. Simulation experiments were also carried out to investigate the effect of applied open gap voltage and interelectrode gap distance on micro-EDM plasma resistance, plasma voltage, current, and the discharge energy. Specific conclusions of the research are as follows:

(1) To solve for the plasma voltage and plasma current during a micro-EDM discharge, plasma was modeled as a simple resistor element to solve the current equation for the EDM pulse-generating circuit. To obtain the resistance of the plasma, dc conductivity of the plasma was used along with the size of the plasma given by the plasma bubble dynamics module.
(2) The model was validated by carrying out single-discharge experiments at open gap voltage of 100 V, interelectrode gap of 1 μm, and pulse-on-time of $t_d = 5$ μs.
(3) From the model predictions, it is seen that the resistance of gap after the plasma formation drops to a value that is almost two orders of magnitude smaller compared to the equivalent impedance of rest of the micro-EDM discharge circuit. This leads to a sharp voltage drop across the electrodes that may be difficult to obtain accurately by a direct measurement due to presence of any stray resistances between the measurement points. Also, due to smaller value of plasma resistance, any stray resistance present between the measurement points across the plasma may lead to overestimation of the actual plasma voltage. As a result, the discharge energy that is going into the plasma during each discharge and causing material removal in micro-EDM may be overestimated as well.
(4) The energy of a discharge is dictated by the resistance of the plasma and the current in the circuit (same as the plasma current). Application of a higher open gap voltage decreases the plasma resistance but increases the plasma current resulting in an increase of the discharge energy for a given gap distance. Whereas, an increase in the interelectrode gap distance increases the plasma resistance but does not affect the plasma current, thereby, increasing the discharge energy at a fixed open gap voltage.
(5) For open gap voltage in the range of 100–300 V and gap distance in the range of 0.5–6 μm, the enhanced model of micro-EDM plasma suggests that a higher open gap voltage and higher interelectrode gap distance can be used to obtain a higher discharge energy, which can lead to a higher MRR [15,19–23]. Also, the predictions of time-transient discharge power can be used in micro-EDM material removal models [23–27] to estimate the heat flux given to the electrodes during a discharge.

Acknowledgment

This material is based in part upon the work supported by the National Science Foundation under Award No. 1033362.

References

[1] Kimoto, Y., 1962, "Study on Erosion Mechanism of Electrical Discharge Machining," J. Inst. Electr. Eng. Jpn, **82**(883), pp. 530–536.
[2] de Bryun, H. E., 1968, "Slope Control—Great Improvement in Spark Erosion," Ann. CIRP, **16**(2), pp. 183–191.
[3] Taniguchi, N., Konoshita, N., and Fukui, M., 1971, "The Optimum Form of the Current Impulse in Electric Discharge Machining," Ann. CIRP, **20**(1), pp. 41–42.
[4] Erden, A., and Kaftanoglu, B., 1981, "Thermo-Mathematical Modeling and Optimization of Energy Pulse Forms in Electric Discharge Machining (EDM)," Int. J. Mach. Tool Des. Res., **21**(1), pp. 11–22.
[5] Rajurkar, K., 1990, "Real-Time Stochastic Model and Control of EDM," CIRP Ann. Manuf. Technol., **39**(1), pp. 187–190.
[6] Kunieda, M., Lauwers, B., Rajurkar, K., and Schumacher, B., 2005, "Advancing EDM Through Fundamental Insight Into the Process," CIRP Ann. Manuf. Technol., **54**(2), pp. 64–87.
[7] Yeo, S. H., Aligiri, E., Tan, P. C., and Zarepour, H., 2009, "A New Pulse Discriminating System for Micro-EDM," Mater. Manuf. Processes, **24**(12), pp. 1297–1305.
[8] Timoshkin, I. V., Fouracre, R. A., Given, M. J., and MacGregor, S. J., 2006, "Hydrodynamic Modelling of Transient Cavities in Fluids Generated by High Voltage Spark Discharges," J. Phys. D: Appl. Phys., **39**(22), pp. 4808–4817.
[9] Lubicki, P., Cross, J. D., Jayaram, S., Staron, J., and Mazurek, B., 1996, "Effect of Water Conductivity on Its Pulse Electric Strength," IEEE International Symposium on Electrical Insulation, Montreal, Canada, June 16–19, Vol. 2, pp. 882–886.
[10] Lan, S., Yang, J., Samee, A., Jiang, J., and Zhou, Z., 2009, "Numerical Simulation of Properties of Charged Particles Initiated by Underwater Pulsed Discharge," Plasma Sci. Technol., **11**(4), pp. 481–486.
[11] Lei, K., Li, N., Huang, H., Huang, J., and Qu, J., 2011, "The Characteristics of Underwater Plasma Discharge Channel and Its Discharge Circuit," *Advanced Electrical and Electronics Engineering* (Lecture Notes in Electrical Engineering), Vol. 87, Springer, Berlin, Heidelberg, pp. 619–626.
[12] Mujumdar, S. S., Curreli, D., Kapoor, S. G., and Ruzic, D., 2014, "A Model of Micro Electro-Discharge Machining Plasma Discharge in Deionized Water," ASME J. Manuf. Sci. Eng., **136**(3), p. 031011.
[13] Lieberman, M. A., and Lichtenberg, A. J., 2005, *Principles of Plasma Discharges and Material Processing*, Wiley, New York.
[14] "Grey-Box Model Estimation," http://www.mathworks.com/help/ident/grey-box-model-estimation.html
[15] Wong, Y., Rahman, M., Lim, H., Han, H., and Ravi, N., 2003, "Investigation of Micro-EDM Material Removal Characteristics Using Single RC-Pulse Discharges," J. Mater. Process. Technol., **140**(1–3), pp. 303–307.
[16] Bragança, I. M. F., Rosa, P. A. R., Dias, F. M., Martins, P. A. F., and Alves, L. L., 2013, "Experimental Study of Micro Electrical Discharge Machining Discharges," J. Appl. Phys., **113**(23), p. 233301.
[17] Kojima, A., Natsu, W., and Kunieda, M., 2008, "Spectroscopic Measurement of Arc Plasma Diameter in EDM," CIRP Ann. Manuf. Technol., **57**(1), pp. 203–207.
[18] Heinz, K., 2010, "Fundamental Study of Magnetic Field-Assisted Micro-EDM for Non-Magnetic Materials," M.S. thesis, University of Illinois at Urbana-Champaign, Champaign, IL.
[19] Gostimirovic, M., Kovac, P., Sekulic, M., and Skoric, B., 2012, "Influence of Discharge Energy on Machining Characteristics in EDM," J. Mech. Sci. Technol., **26**(1), pp. 173–179.
[20] Daneshmand, S., and Kahrizi, E., 2013, "Influence of Machining Parameters on Electro Discharge Machining of NiTi Shape Memory Alloys," Int. J. Electrochem. Sci., **8**(3), pp. 3095–3104.
[21] Kiyak, M., Aldemir, B. E., and Altan, E., 2015, "Effects of Discharge Energy Density on Wear Rate and Surface Roughness in EDM," Int. J. Adv. Manuf. Technol., **79**(1), pp. 513–518.

[22] Jahan, M. P., Ali Asad, A. B. M., Rahman, M., Wong, Y. S., and Masaki, T., 2011, "Micro-Electro Discharge Machining," *Micro-Manufacturing: Design and Manufacturing of Micro-Products*, 1st ed., M. Koc and T. Ozel, eds., Wiley, Hoboken, NJ, pp. 301–346.
[23] Tao, J., Ni, J., and Shih, A. J., 2012, "Modeling of the Anode Crater Formation in Electrical Discharge Machining," ASME J. Manuf. Sci. Eng., **134**(1), p. 011002.
[24] Yeo, S. H., Kurnia, W., and Tan, P. C., 2007, "Electro-Thermal Modelling of Anode and Cathode in Micro-EDM," J. Phys. D: Appl. Phys., **40**(8), pp. 2513–2521.
[25] Yeo, S. H., Kurnia, W., and Tan, P. C., 2008, "Critical Assessment and Numerical Comparison of Electro-Thermal Models in EDM," J. Mater. Process. Technol., **203**(1–3), pp. 241–251.
[26] Joshi, S., and Pande, S., 2010, "Thermo-Physical Modeling of Die-Sinking EDM Process," J. Manuf. Processes, **12**(1), pp. 45–56.
[27] Mujumdar, S. S., Curreli, D., Kapoor, S. G., and Ruzic, D., 2015, "Modeling of Melt-Pool Formation and Material Removal in Micro-Electrodischarge Machining," ASME J. Manuf. Sci. Eng., **137**(3), p. 031007.